s dependence of proton fragmentation by hadrons. I. Incident laboratory momenta 4–24 GeV/c

E. Beier, H. Brody, G. Featherston,* D. Kreinick,† R. Patton, K. Raychaudhuri, H. Takeda, R. Thern, R. Van Berg, and H. Weisberg‡

Department of Physics, University of Pennsylvania, Philadelphia, Pennsylvania 19104

(Received 2 December 1977)

Measurements of the dependence on $s = (p_a + p_b)^2$ of the cross sections for production of single charged hadrons in the reactions $a + b \to c +$ anything are presented. Particle c was detected in a fixed interval of laboratory momentum and angle in the fragmentation region of the target proton. The $\pi^{\pm}$ and K^+ production data are consistent with the Mueller-Regge prediction of an approach to scaling as $A + Bs^{-1/2}$. Further tests of a simple Regge-pole model indicate that the s dependence measured is fortuitous, and that higher-energy data are required in order to make detailed tests of the model.

I. INTRODUCTION

In recent years the approach to a conjectured scaling limit in the single-particle hadron inclusive reactions $a+b \to c+$anything has received considerable experimental and theoretical attention.[1] This paper reports the results of a systematic study of the dependence of these reactions on $s=(p_a+p_b)^2$ for particle types $a=(\pi^{\pm},K^{\pm},p^{*})$, $b=p$, and $c=(\pi^{\pm},K^{+},p)$. The particles of type c are detected in a small, fixed region of phase space in the laboratory corresponding to small laboratory momentum. The measurements were made at incident momenta $p_a=4$, 6, 8, 10, 12, 15, 20, and 24 GeV/c.

The Mueller-Regge phenomenology[2,3] provides a framework for interpretation of these data. This phenomenology predicts that for sufficiently large values of s the cross sections for production of particles which have low momenta in the laboratory will depend on s according to $A+Bs^{-1/2}$, where A and B are functions of $\vec{p}_c$, but not of s. The data presented here are used to test this prediction, along with more detailed predictions such as Pomeron factorization.

In Sec. II the kinematic region under investigation is specified and the phenomenology associated with this region is summarized. Section III presents a discussion of the experimental technique. Section IV discusses the computation of the cross sections with emphasis on the calibration of the absolute normalization. In Sec. V the results of the measurements are presented and interpreted.

II. KINEMATICS AND PHENOMENOLOGY

In this experiment, data on the inclusive production of a single particle c in the hadron interactions $a+p \to c+$anything were taken at fixed angle and momentum in the laboratory as the incident momentum was varied. The limits of the acceptance of the spectrometer used to measure particle c were

$$59.4^\circ \leq \theta_c^{\rm lab} + 3.4^\circ[(\text{GeV}/c)/(p_c^{\rm lab} - \Delta p_c)] \leq 64.4^\circ$$

and (1)

$$0.3 \text{ GeV}/c \leq p_c^{\rm lab} - \Delta p_c \leq 0.6 \text{ GeV}/c,$$

where $\Delta p_c \simeq (0.0015 \text{ GeV}/c)/\beta_c^3$ is the momentum lost by particle c before the momentum measurement and β_c is its velocity.

This region of $p_c^{\rm lab}$, $\theta_c^{\rm lab}$ is shown in Fig. 1(a), and the same region, expressed in transverse momentum and laboratory rapidity, is shown in Fig. 1(b). In this kinematic range the transverse momentum of particle c is typically $p_\perp=0.3$ GeV/c and the laboratory rapidity is $y_L=0.6$, 0.4, and 0.2 for produced π, K, and p, respectively. Particles with such small momenta in the rest frame of the target proton and referred to as fragments of the target.

According to Mueller,[2] the invariant cross section for single-particle production in the reaction $a+b \to c+$anything is related to a particular discontinuity in the amplitude for forward scattering of the $ab\bar{c}$ system as indicated pictorially in Fig. 2(a). Mueller further argues that in the target fragmentation region where $u=(p_b-p_c)^2$ is small this amplitude can be represented by the sum of single Regge exchanges between the system $b\bar{c}$ and particle $\bar{a}$ as indicated pictorially in Fig. 2(b). The invariant cross section then is represented by

$$E\frac{d^3\sigma}{d^3p} = \beta_{b\bar{c}}^{P}(p_\perp,y_L)\gamma_a^P s^{\alpha_P(0)-1} + \sum_R \beta_{b\bar{c}}^{R}(p_\perp,y_L)\gamma_a^R s^{\alpha_R(0)-1}, \quad (2)$$

where $\beta_{b\bar{c}}^{R,P}(p_\perp,y_L)$ is the coupling of the Reggeon or Pomeron to the $b\bar{c}$ system at a definite y_L and $p_\perp$, and $\gamma_a^{R,P}$ is the Reggeon or Pomeron coupling

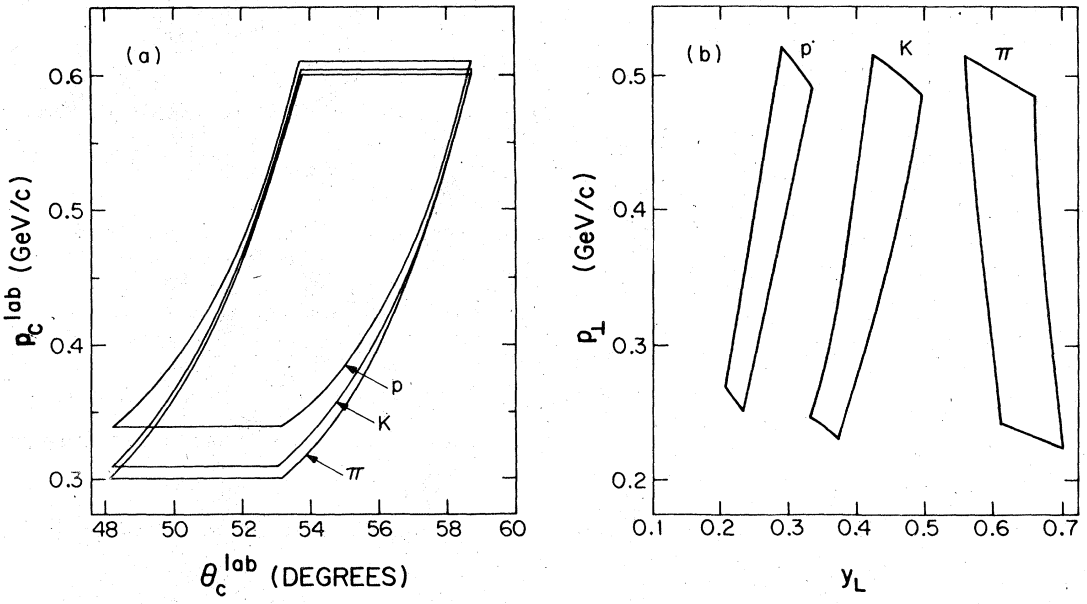

FIG. 1. (a) Limits of the spectrometer acceptance in laboratory momentum p_c^{lab} and laboratory angle θ_c^{lab}. The boundaries are different for produced π, K, and p due to differences in momentum loss before the momentum measurement, as described in Eq. (1). (b) Same limits of spectrometer acceptance expressed in transverse momentum $p_\perp$ and laboratory rapidity y_L of particle c.

to particle a at zero-momentum transfer. It is usually assumed for phenomenological analysis that the Pomeron is a factorizable pole with intercept $\alpha_P(0)=1$. With $\alpha_R(0)<1.0$, the relation $\alpha_P(0)=1.0$ makes the invariant cross section become a constant at large s, in accord with the hypothesis of limiting fragmentation.[1]

The expression for the invariant cross section is further simplified by including only the vector and tensor meson trajectories ρ, ω, A_2, and f which have the next highest intercepts $\alpha_R(0)\approx 0.5$. The invariant cross section then assumes the simple form

$$E\frac{d^3\sigma}{d^3p}=A(p_\perp,y_L)+B(p_\perp,y_L)s^{-1/2}. \tag{3}$$

Using the optical theorem, a similar expression can be obtained for the total cross section for particle a scattering on particle b,

$$\sigma_T(ab)=\gamma_a^P\gamma_b^P s^{\alpha_P(0)-1}+\sum_R \gamma_a^R\gamma_b^R s^{\alpha_R(0)-1}, \tag{4}$$

where the coupling strengths $\gamma_a^{R,P}$ are the same as in Eq. (2). At asymptotic energies, only the Pomeron term contributes to Eq. (2) and Eq. (4). Pomeron factorization can be tested by comparing the ratio of cross sections for production of particle c by two different particles a and a' with the ratio of the total cross sections for particles a and a' in the limit $s^{-1/2}\to 0$:

$$\lim_{s^{-1/2}\to 0}\frac{E(d^3\sigma/d^3p)(a'+b\to c+x)}{E(d^3\sigma/d^3p)(a+b\to c+x)}=\frac{\gamma_{a'}^P}{\gamma_a^P}=\lim_{s^{-1/2}\to 0}\frac{\sigma_T(a'b)}{\sigma_T(ab)} \tag{5}$$

Charge-conjugation invariance of the particle-

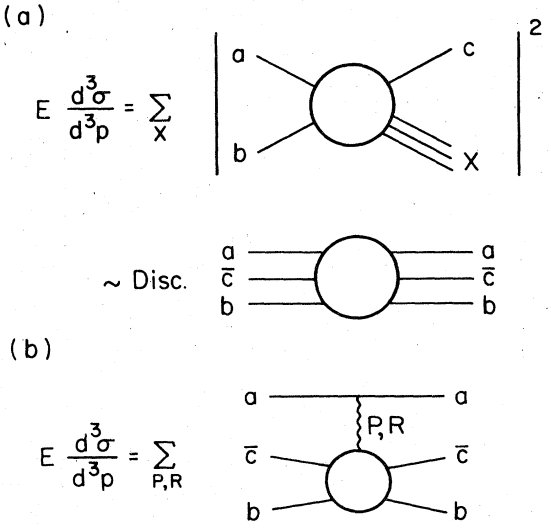

FIG. 2. (a) Pictorial representation of the Mueller theorem. (b) Pictorial representation of the application of the Mueller theorem to the fragmentation region of particle b using a simple Regge-pole model.

Reggeon coupling leads to relations between the production of particle c by particle a and its antiparticle $\bar{a}$.[3] Of specific interest here are the π^+,π^- induced reactions:

$$E\frac{d^3\sigma}{d^3p}(\pi^+ + p \to c + x) = A_P - B_\rho s^{\alpha_\rho(0)-1} + B_f s^{\alpha_f(0)-1},$$
$$E\frac{d^3\sigma}{d^3p}(\pi^- + p \to c + x) = A_P + B_\rho s^{\alpha_\rho(0)-1} + B_f s^{\alpha_f(0)-1}. \quad (6)$$

The difference of these two cross sections has an s dependence which is a power law determined by the intercept of the ρ trajectory.

III. EXPERIMENTAL TECHNIQUE

A. Beam

The experiment was performed at the Brookhaven National Laboratory Alternating Gradient Synchrotron in the 0° charged beam at target station B. The beam is shown in Fig. 3. It has two approximately symmetric sections with an intermediate focus in both planes. The momentum dispersion at the first focus was 0.6% per centimeter; the second section provided momentum recombination at the final focus.

Beam particles entering the 20-cm-long × 3.8-cm-diameter liquid hydrogen target at the final focus were defined by a triple coincidence between scintillation counters $B1$, $B2$, and $B3$. Counter $B3$ was 2.5 cm in diameter, centered on the target axis, and located 24 cm upstream from the center of the target. Counters $B1$ and $B2$ were located immediately upstream from dipole magnet $D3$ and immediately downstream from quadrupole magnet $Q9$, respectively. The beam-spot size at the final focus was approximately 0.7 cm rms horizontally and vertically at momenta above 8 GeV/c, and was somewhat larger at lower momenta due to multiple scattering.

Four threshold Čerenkov counters were used to identify the types of particles in the beam. At beam momenta of 8 GeV/c and above two counters, $\pi 1$ and $\pi 2$, were set to count pions, and two others, $K1$ and $K2$, were set to count both pions and kaons. The following signals were generated:

$$\begin{aligned} B &= B1 \cdot B2 \cdot B3, \\ \pi &= B \cdot \pi 1 \cdot \pi 2 \cdot (K1 + K2), \\ K &= B \cdot (\overline{\pi 1 + \pi 2}) \cdot K1 \cdot K2, \\ p &= B \cdot (\overline{\pi 1 + \pi 2 + K1 + K2}). \end{aligned} \quad (7a)$$

At 4 and 6 GeV the counters $\pi 1$ and $\pi 2$ were not used. The electronic logic was modified to generate the signals:

$$\begin{aligned} \pi &= B \cdot K1 \cdot K2, \\ p &= B \cdot (\overline{K1 + K2}) \text{ (positive beam only).} \end{aligned} \quad (7b)$$

The K^+ contamination of the proton signal was less than 2% at 4 and 6 GeV/c. No correction was made for this contamination.

The signals were counted in scalers to measure the flux of each particle type and were stored in latches for each event trigger, thus determining the incoming-particle type for each event. The individual Čerenkov-counter signals also stopped time to digital converters which each event trigger started. This information was used to study the contamination due to misidentification of hadrons and the accidental coincidences in the π, K, and p signals above. It was determined that no such corrections to the recorded π, K, and p fluxes were required.

The π signal was contaminated by leptons (e and μ) in the beam. This background was measured by performing pressure curves with the beam Čerenkov counters at each momentum. The measured contamination ranged from 6% at 6 GeV/c to less than 1% above 12 GeV/c, and was subtracted from

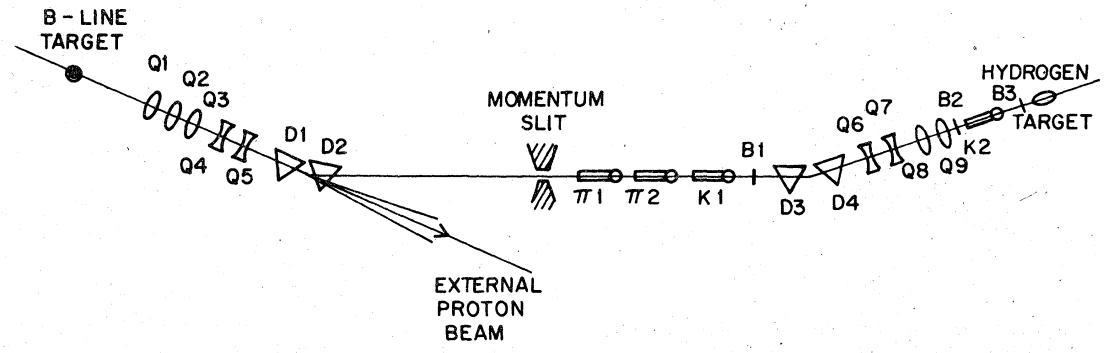

FIG. 3. Layout (not to scale) of the unseparated charged-particle beam. $D1$–4 are dipole magnets, $Q1$–9 are quadrupole magnets, $B1$–3 are scintillation counters, and $\pi 1$, $\pi 2$, $K1$, $K2$ are threshold Čerenkov counters.

the π signal. It was further observed that insertion of 1.5 radiation lengths of lead at the intermediate focus of the beam reduced the electron contamination by at least a factor of 100 with negligible effect on other particle types. Later runs were made with this lead in place.

B. Spectrometer

The spectrometer, shown schematically in Fig. 4, utilized a single dipole, which was a C magnet with 30.5-cm × 61.0-cm poles and a 10.2-cm gap. Eighteen planes of multiwire proportional chambers (PWC) defined the trajectory of the particle; scintillation and Čerenkov counters identified the particle type. Two scintillation counters, $T1$ and $T2$, in coincidence defined a particle traversing the spectrometer. The event trigger was a coincidence between a beam particle and a particle traversing the spectrometer, $B \cdot T = (B1 \cdot B2 \cdot B3) \cdot (T1 \cdot T2)$. The solid-angle acceptance of the spectrometer was approximately 3 msr, the momentum acceptance, approximately one-half the central momentum, and the momentum resolution, typically 1%. The entire spectrometer was constructed on a steel beam which pivoted about a point directly beneath the hydrogen target. This feature allowed the spectrometer to be moved into the beam to calibrate PWC positions and the zero scattering angle, or to be moved to the elastic-scattering limit to check the secondary-particle-momentum calibration and the cross-section absolute normalization.

The cross section for the production of particles of a given angle, momentum, and particle type was measured as the product of two factors. The first factor is the cross section for production of charged particles of all types, which was measured in the section of the spectrometer from the target up to scintillator $T2$. (This section has low mass and hence small scattering and absorption corrections.) The second factor is the ratio of particles of a given type to all charged particles of given momentum and angle; this ratio was measured in the section of the spectrometer including scintillators $T2$ and $T3$, Čerenkov counter $C1$, and the last two planes of PWC. With this technique, systematic corrections for scattering and absorption of secondary particles are typically much smaller than in measurements made with spectrometers which have the acceptance defining counters preceded by Čerenkov counters.

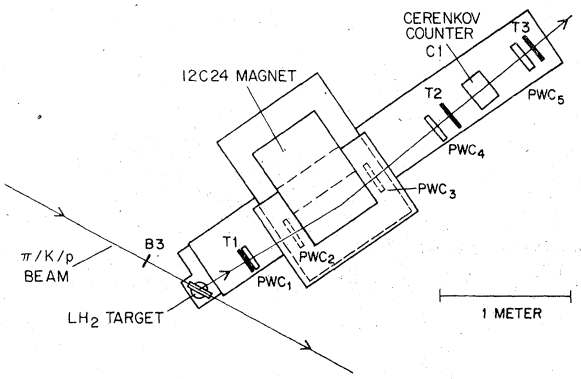

FIG. 4. Layout of the spectrometer. $B3$, $T1$, $T2$, and $T3$ are scintillation counters, $C1$ is a threshold Čerenkov counter, and PWC_{1-5} are multiwire proportional chamber modules.

The multiwire proportional chambers were of conventional design, with approximately 0.48-cm gap spacing and 0.2-cm anode wire spacing. The anodes were constructed from 20-μ stainless steel wire and the cathodes from 7.6-μ aluminum foil. The gas was a mixture of approximately 73% Argon, 22% isobutane, 0.5% Freon 13B1, and 4% methylal. Two modules of four planes (X, Y, W, X) were placed on each side of the magnet to measure the particle momentum, and a fifth module of two planes (X, Y) was placed behind the particle identification detectors to measure the interactions in these detectors. The wires in all Y and W planes, and the X plane of the fifth module, were OR'ed in pairs at the chamber with an attendant loss of resolution and increase in economy.

Individual wires adjacent to a particle trajectory produced signals which were amplified by μA760 comparator circuits, electronically delayed by SN74121 monostable multivibrators, reshaped, and strobed into SN7494 parallel in, serial out shift registers by a coincidence with the event trigger $B \cdot T$. The same event trigger also interrupted a PDP-9 control computer which initiated a scan of the PWC registers. The shift registers in each module of PWC were connected as one large serial shift register. A local clock at each module shifted the data and incremented an address register until an address corresponding to a "hit" wire was found, at which time a flag requesting service was raised.. A central scanner at the PDP-9 sequentially polled the local scanners at each module, transferring a 12-bit address from each local scanner which had data to transfer. When three 12-bit words accumulated in the central scanner, they were read into the PDP-9 as two 18-bit words. Pulse height, time of flight, and latch information from the event was read from standard CAMAC instrumentation.

The PDP-9 was arranged to have two 2070_8 word magnetic tape buffers. Each full buffer contained approximately 20 events, one record with all of the CAMAC scaler information, and certain control and monitoring information. Each full buffer was

written, along with a checksum, as one physical record on magnetic tape. Each such record was an independent unit of data, and no error resulted if one or more records were lost because of data recording errors. While the full buffer was being written on magnetic tape, data accumulated in the second buffer. The maximum data rate for the experiment was about 250 events/sec and was limited by the speed of the magnetic tape drive. The data reported here were collected at typically one-tenth of the maximum rate.

The first PDP-9 buffer written in any accelerator cycle was also transferred to a Brookhaven On-Line Data Facility PDP-10 for event reconstruction and analysis. Much of the analysis described in this paper was performed on-line on a sample of the data. This proved to be an indispensable monitor of the performance of the experiment.

The event reconstruction algorithm required that three of the four Y and W planes and three of the four X planes in front of, and behind, the magnet be present. The track was first determined in the nonbending Y plane, and then the correlation was made with track segments before and after the magnet in the bend plane (X plane). Slopes of the trajectory were computed on either side of the magnet, and from these the momentum and production angle of the particle were determined.

The efficiency of the reconstruction algorithm was studied using Monte Carlo data and was greater than 0.99. Since the event reconstruction was redundant, the PWC efficiency could be studied by examining individual tracks in the actual data sample. (Tracks made by slow particles were not used in this test since they had greater ionization and correspondingly higher PWC efficiency.) Individual dead wires and average plane inefficiencies were monitored in this way, and an estimated reconstruction inefficiency was calculated and applied to the data. This correction was typically about 1%.

From the measured momentum and the time of flight from $B3$ to scintillation counters $T2$ and $T3$, the mass squared distribution at each of these counters was constructed for particles traversing the spectrometer. It can be seen in Fig. 5(a) that the resolution at $T2$ identifies the protons uniquely. The vertical lines in the figure represent the cuts used to define the proton sample. The tails of the distribution indicate a background which receives contributions from (1) events which scatter in the spectrometer in such a way that the measured momentum does not match the time of flight, (2) events with extra "hits" in the front chambers which are not properly reconstructed by the pattern recognition algorithm, and (3) secondary particles produced by beam particles which come after another beam particle but within the time resolution of the B telescope. The systematic error in the quoted cross sections from ignoring these backgrounds is less than 1%.

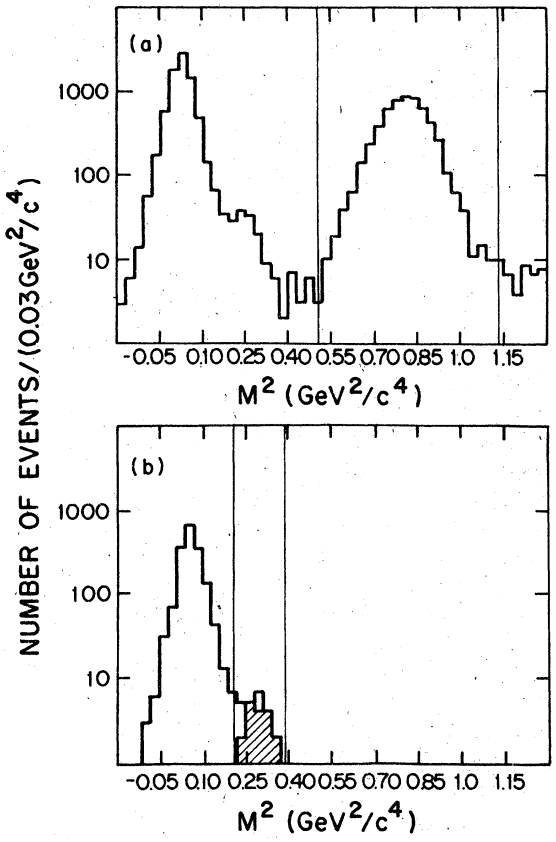

FIG. 5. (a) Distribution of mass squared constructed from momentum and time of flight to scintillator $T2$. Events between the vertical lines define the proton sample; events with $M^2 < 0.5$ GeV^2 define the sum of the pion and kaon smaple. (b) Distribution of mass squared constructed from momentum and time of flight to scintillator $T3$ (excluding protons). The shaded events did not produce a signal in Čerenkov counter $C1$ and are defined to be kaons when they lie between the vertical lines.

Threshold Čerenkov counter $C1$ was used in separating pions from kaons. This counter utilized a 3.8-cm-thick × 21.6-cm-diameter radiator cell containing liquid $FC75$, a fluorocarbon with index of refraction $n = 1.28$. It counted pions but not kaons in the momentum range studied. Čerenkov light produced in the cell was reflected in a 10-cm-long × 30-cm-diameter cylinder painted with Eastman white reflectance paint number 6080, and viewed by four 12-cm-diameter photomultiplier tubes. The pulse heights in these tubes were added off-line to determine the counter response.

The pion-kaon separation was made only for events which reconstructed at PWC_5. In this way, misidentifications caused by interactions in the Čerenkov counter or $T2$ were eliminated. Signals from knock-on electrons were rejected by a pulse-height requirement in $C1$. The response of $C1$ was tested on pure pion and proton samples defined by time-of-flight and energy-loss requirements in $T2$ and $T3$. The efficiency was found to be greater than 99% for pions and less than 1% for protons.

Figure 5(b) shows the mass-squared distribution at $T3$ for the pion and kaon sample, defined by low mass squared in $T2$, reconstruction in PWC_5, and a signal in $T3$. The subsample that produced a signal below the pulse-height requirement in $C1$ is shown as the shaded events in Fig. 5(b). Note that the pion rejection is large, since all events in the peak produced a signal in $C1$. The kaon signal is quite clear, and is defined by the vertical lines. The kaon fraction of the low-mass particles was thus determined. From it the pion fraction of the low-mass particles was then determined by subtraction, in a manner which is insensitive to small changes in the efficiencies of $C1$, $T3$, and PWC_5. Contributions to the low-mass particle flux from electrons and muons were calculated to be negligible.

The measured kaon-to-pion ratio at $T3$ was corrected for interactions and decays between $T2$ and $T3$ to produce the kaon-to-pion ratio at $T2$. The decay corrections were determined by a Monte Carlo calculation. For pions the interaction correction was determined experimentally by adding additional absorbers between $T2$ and $T3$. In addition, both the pion and kaon interaction corrections were calculated using data on cross sections in complex nuclei. Agreement between the measured and calculated pion absorption provides confidence in the calculated kaon absorption. Further, because the pion–to–pion-plus-kaon ratio is close to unity, the fractional uncertainty in the pion cross section is quite small. Although the systematic uncertainties in the kaon ratio are larger, knowledge of the cross section is ultimately limited by statistics.

IV. ANALYSIS

The spectrometer measures the number of particles of each particle type which are produced within its momentum and solid angle acceptance. This section describes the calculation of absolute cross sections from these raw rates and consistency checks performed on the data.

The intensity dependence of the rate of single-charged-particle production was studied by varying the intensity of the incident beam while holding all other conditions fixed. The production rate, with empty-target background subtracted, was measured to a sensitivity of 2% to be independent of the intensity of the incoming beam. The intensity of the incident beam for all the data discussed in this paper was approximately 2×10^6 particles/sec.

The same production rate was measured as a function of the horizontal displacement of the beam. The measured production rate was independent of small drifts in the horizontal bending magnet currents to a sensitivity of 3%. The magnet current drift which generated an alarm from the readings of the digital voltmeter monitoring the magnet shunts corresponded to about 0.7 cm horizontal displacement, which was equal to the rms size of the beam and much smaller than the liquid hydrogen target.

The vertical distribution of tracks reconstructed in the spectrometer and extrapolated back to the liquid hydrogen target monitored vertical drifts of the beam. These drifts correspond to changes in the vertical position of the primary production target of the beam. Because the production target was small and the magnification of the beam was approximately unity, such vertical drifts were

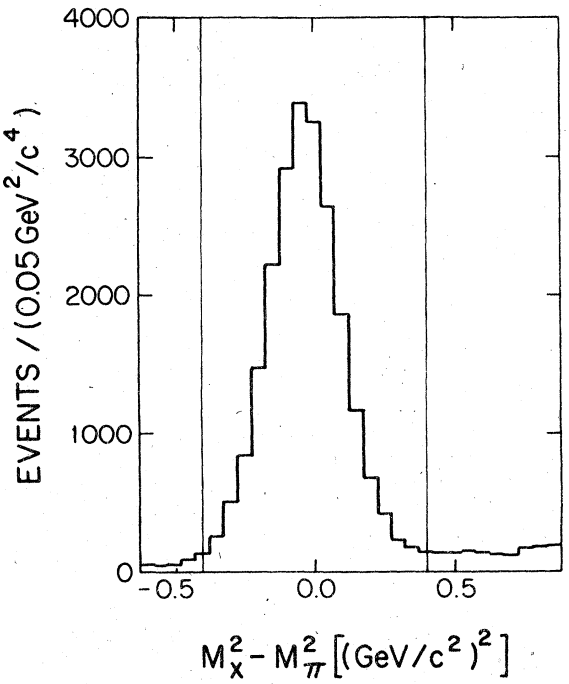

FIG. 6. Distribution of missing mass squared minus pion mass squared for 13-GeV/c π^-p elastic scattering events in the range $0.18 < -t < 0.4$ GeV^2. The vertical lines define the sample of elastic scattering events. The asymmetry in the distribution is caused by the spectrometer acceptance.

negligible.

The acceptance corrections were tested on both Monte Carlo–generated and real elastic scattering events. The acceptance is a function of the scattering angle θ, the momentum p, and the longitudinal position z of the interaction in the target. A fiducial area at scintillation counter $T2$ defined the acceptance. A computer program was used to trace rays of definite θ, p, and z through the spectrometer to the plane of $T2$; the azimuthal angle φ of the ray was varied until the ray intersected the boundary of the fiducial area. These values of φ, corresponding to the boundary of the fiducial area at $T2$, defined the acceptance function $\Delta\Phi(\theta,p,z)$.

Two methods were used to calculate the elastic differential cross sections. The first method required that the bins of scattering angle θ be small enough that the differential cross section $d\sigma/dt$ did not change much over the bin width $\Delta\theta$. The differential cross section is then defined by the equation

$$n_d = n_i \rho N_0 \frac{d\sigma}{dt}\frac{\Delta t}{\Delta\theta}\int_{\theta_1}^{\theta_2} d\theta \int_{z_1}^{z_2} dz \frac{\Delta\Phi(\theta,p(\theta)-\Delta p,z)}{2\pi}, \tag{8}$$

where

n_d = number of elastic events in $\Delta\theta$,
n_i = total number of incident particles,
ρ = density of liquid hydrogen,
N_0 = Avogadro's number,
$\Delta\theta = \theta_2 - \theta_1$,
$\Delta t = t(\theta_2) - t(\theta_1)$,
Δp = momentum lost before the magnet,
$p(\theta) = 2m_p\beta\cos\theta/(1-\beta^2\cos^2\theta)$, momentum defined by elastic kinematics,
$\beta = p_a/(E_a + m_p)$, where p_a and E_a are the momentum and energy of the incident particle, and m_p is the proton mass.

The second method used the measured momentum and weighted each event by the acceptance integrated over target position. The differential cross section for this case is given by

$$\frac{d\sigma}{dt} = \frac{1}{n_i}\frac{1}{\rho N_0}\frac{2\pi}{\Delta t}\sum_i W_i, \tag{9}$$

where

$$W_i = \frac{1}{\int_{z_1}^{z_2} dz\,\Delta\Phi(\theta_i,p_i,z)}.$$

The sum is over all events which satisfied the missing-mass requirement for elastic scattering (see below) and which have $\theta_1 < \theta_i < \theta_2$.

The two methods of analyzing elastic scattering data were applied to a sample of Monte Carlo events which were generated from a parent distribution Be^{7t} and traced through the spectrometer. The two methods of analysis reproduced the parent distribution well.

Real elastic scattering data were obtained for the reaction $\pi^- p \to \pi^- p$ at 13 GeV/c at two settings of spectrometer angle having overlapping acceptance. Figure 6 shows the distribution of missing mass squared and the cuts used to define the sample of elastic scattering events. The cross sections calculated by each method of analysis were in excellent agreement. The experimental differential cross section for the second method of analysis with empty-target subtraction and absorption corrections of about 2% is displayed in Fig. 7 together with results from another experiment.[4] The agreement between the two methods of analysis shows that the momentum calibration of the spectrometer is correct; the agreement with other experiments shows that the calculation of the acceptance function is correct.

The inelastic cross sections quoted in this paper are differential cross sections integrated over the phase-space acceptance, A, of the spectrometer, defined in Eq. (1), and integrated over all azimu-

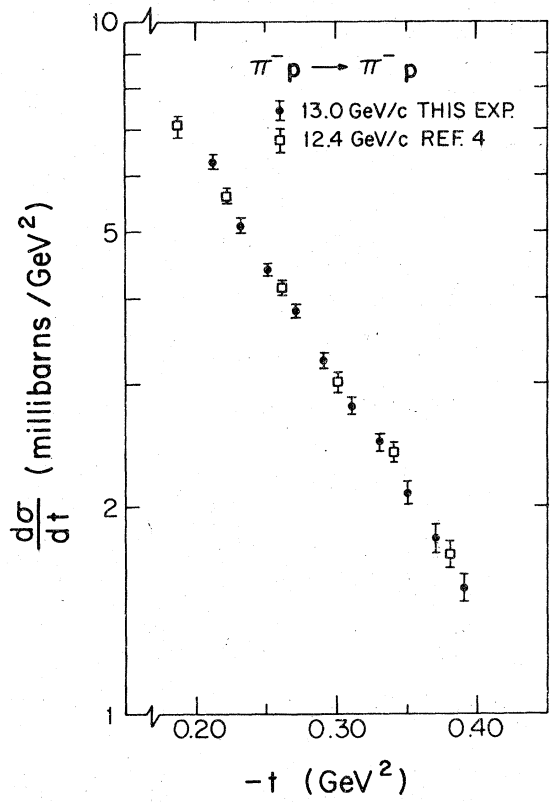

FIG. 7. Differential cross section for $\pi^- p$ elastic scattering at 13 GeV/c.

thal angles:

$$\Delta\sigma = \int_0^{2\pi} d\varphi \int_A d\theta\, dp\, \frac{d^3\sigma}{d\theta dp d\varphi} . \quad (10)$$

This expression is equivalent to integrating the invariant differential cross section $d^2\sigma/dy dp_\perp^2$ over the invariant-phase-space acceptance [Fig. 1(b)] of the spectrometer.

The inelastic cross sections were obtained from a formula which is analogous to that for the second method of determining the elastic cross sections:

$$\Delta\sigma = \frac{1}{n_i} \frac{2\pi}{\rho N_0} \sum_i W_i . \quad (11)$$

The notation is the same as previously introduced, and the sum is over all events having θ_i and p_i within the spectrometer acceptance defined in Eq. (1). Corrections affecting the absolute normalization of the inelastic cross sections are the decay factor for decays between the production point and $T2$, and absorption of the beam in the liquid hydrogen target and in scintillation counter $B3$. The decay factor is momentum dependent (and to a good approximation θ independent) and was computed by a Monte Carlo calculation. It is included in the weight W_i on an event-by-event basis, and averages about 10% for pion production and 100% for kaon production. The absorption of secondary particles was calculated as a function of momentum from total-cross-section data. It also is included in W_i and averages about 1.5%. The beam flux was taken to be the scaler reading for a given particle type reduced by a factor to give the flux halfway through the liquid hydrogen. This correction depends on particle type and is typically a few per cent. Owing to the small amount of material between the hydrogen target and $T2$, the corrections for multiple scattering are negligible.

The absolute calibration of the inelastic cross section was checked by integrating a local fit to the data of Ref. 5 on the reactions $pp \to \pi^\pm$ at 12 GeV/c over the acceptance region defined in Eq. (1). From Ref. 5, the integrated cross sections for $pp \to \pi^+$ (π^-) are 0.439 ± 0.007 mb (0.204 ± 0.003 mb). From this experiment the cross sections for $pp \to \pi^+$ (π^-) are 0.440 ± 0.006 mb (0.210 ± 0.004 mb).

V. RESULTS AND CONCLUSIONS

The invariant cross sections, integrated over the acceptance of the apparatus, are displayed for π^-, π^+, K^+, and p production in Figs. 8(a)–8(d) as a function of $s^{-1/2}$. The error bars shown correspond to statistical errors added in quadrature with an estimated 2% point-to-point systematic error. In addition, we estimate that there is an overall normalization uncertainty of 3% for pion and proton production and 15% for kaon production. Numerical values are given in the following paper.[6]

Production of K^- and $\bar{p}$ are below the limit of sensitivity of this experiment, and no conclusions about their cross sections can be made. For the reactions where particles a and c are $\pi^\pm$ or p, the errors are typically smaller than the symbols on the graphs.

The pion production reactions, Figs. 8(a) and 8(b), are well parametrized by $A + Bs^{-1/2}$ for $p_a^{\rm lab} \geq 6$ GeV/c. For production of protons, Fig. 8(d), the missing mass at the lowest beam momentum is in the resonance region rather than the deep-inelastic region. Indeed, there is a prominent peak in $\pi^\pm p \to p$ at 6 GeV/c corresponding to $\pi^\pm p \to A_2^\pm p$, although the data are consistent with the onset of $A + Bs^{-1/2}$ behavior at higher momenta.

The solid straight lines in Figs. 8(a)–8(c) correspond to fits of the $\pi^\pm$ and K production data to $A + Bs^{-1/2}$ for $p_a^{\rm lab} \geq 6$ GeV/c with the additional constraint that the intercept A at $s^{-1/2} = 0$ is the same for particle- and antiparticle-induced reactions. The parameters of the fit are tabulated in Table I. From Figs. 8(a)–8(d) and Table I we con-

TABLE I. $A + Bs^{-1/2}$ fits to the data for produced $\pi^\pm$ and K^+. The fits were carried out over the momentum range $6 \leq p_a^{\rm lab} \leq 24$ GeV/c.

Reaction	A (μb)	B (μb GeV)	χ^2	DF
$\pi^- p \to \pi^-$		668 ± 59		
	117 ± 12		6.4	9
$\pi^+ p \to \pi^-$		158 ± 52		
$K^- p \to \pi^-$		180 ± 395		
	126 ± 78		7.4	7
$K^+ p \to \pi^-$		-126 ± 354		
$\bar{p} p \to \pi^-$		1509 ± 270		
	360 ± 16		4.7	7
$pp \to \pi^-$		-720 ± 73		
$\pi^- p \to \pi^+$		267 ± 65		
	225 ± 14		17.0	10
$\pi^+ p \to \pi^+$		792 ± 63		
$K^- p \to \pi^+$		382 ± 550		
	153 ± 110		5.7	7
$K^+ p \to \pi^+$		417 ± 526		
$\bar{p} p \to \pi^+$		907 ± 284		
	532 ± 27		9.5	8
$pp \to \pi^+$		-459 ± 127		
$\pi^- p \to K^+$		-1.1 ± 8.9		
	5.0 ± 1.9		12.6	11
$\pi^+ p \to K^+$		-1.0 ± 8.3		
$pp \to K^+$	6.8 ± 2.7	-7.9 ± 14.1	3.8	6

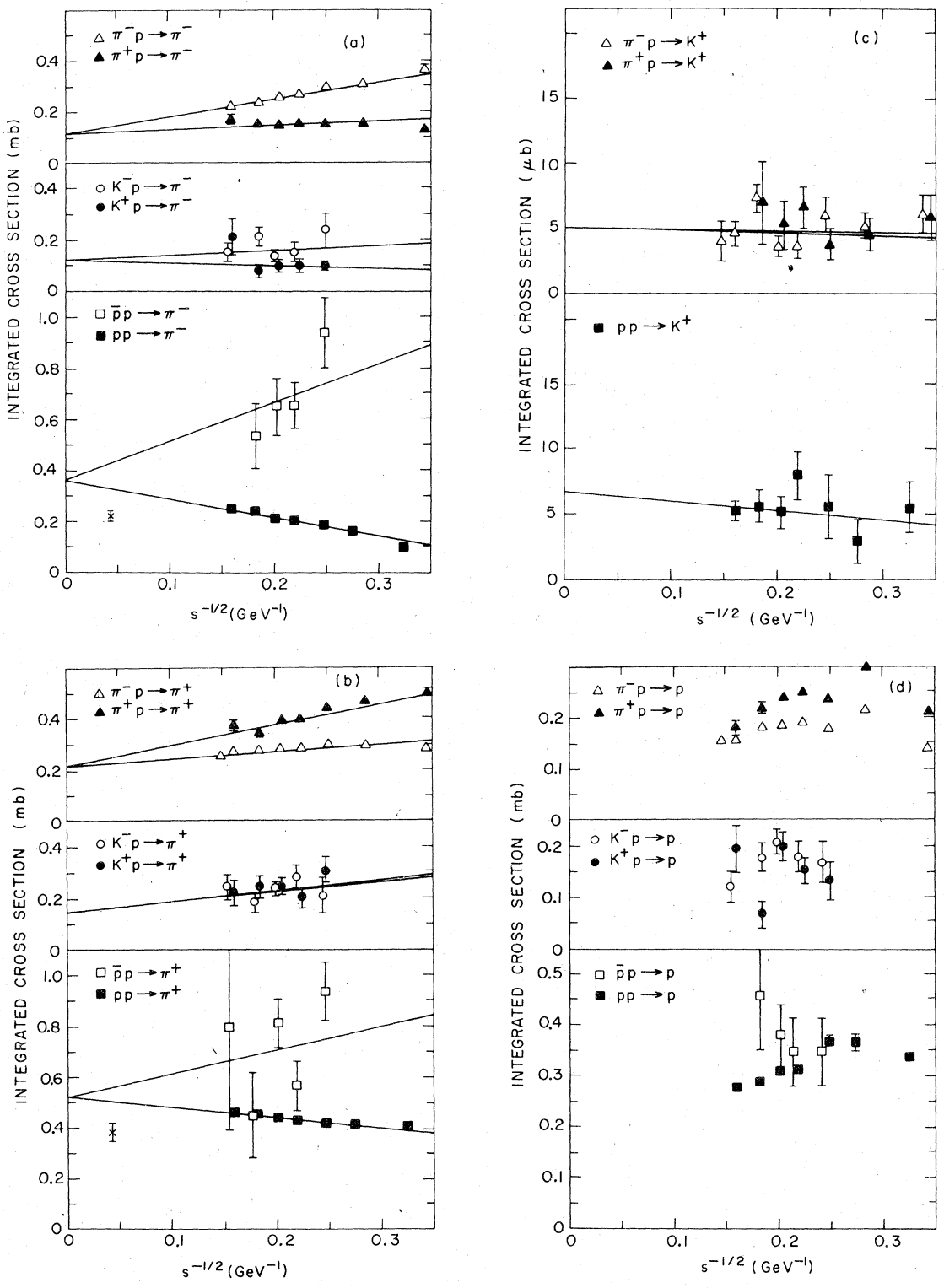

FIG. 8. Cross sections, integrated over the kinematic region in Eq. (1), for the production of (a) π^-, (b) π^+, (c) K^+, and (d) p. The solid lines are fits to $A + B\, s^{-1/2}$ for $6 \leq p^a_{\rm lab} \leq 24$ GeV/c as given in Table I. Where two symbols overlap, the negative-beam symbol has been displaced to the left. The points at $s^{-1/2} \approx 0.04$ for the reactions $pp \to \pi^\pm$, indicated by the symbol $X_{\bar{3}}$, are deduced from Ref. 10.

clude that in the region of phase space measured in this experiment we have the following:

(a) The cross sections for $pp \to \pi^{\pm}$, $\pi^- p \to \pi^{\pm}$, and $\pi^+ p \to \pi^-$ are remarkably well fitted by $A + Bs^{-1/2}$; those for $\pi^+ p \to \pi^+$ are less well fitted by this form.

(b) The cross sections for $pp \to \pi^{\pm}$ increase with s in this range of s. Other cross sections with strong s dependence decrease with increasing s.

(c) The π^+ and π^- induced pion production cross sections approach each other as s increases for both signs of secondary pions.

(d) The cross sections for π^+ production by K^+ and K^- are approximately the same. The cross sections for π^- production by K^+ and K^- differ by a factor of 2, implying that at least one of these cross sections has a large s dependence.

The success of the fits to the expression $A + Bs^{-1/2}$ suggests that data in this range of s should be compared with the detailed predictions of the Mueller-Regge phenomenology, as developed in Sec. II.

Pomeron factorization implies that the ratio of intercepts A_p/A_π for the reactions $pp \to c$ and $\pi p \to c$ should be the same as the ratio of the total cross sections $\sigma(pp)/\sigma(\pi p)$. The ratio $[\sigma_T(\bar{p}p) + \sigma_T(pp)]/[\sigma_T(\pi^+ p) + \sigma_T(\pi^- p)]$ at 200 GeV/c from Ref. 7 is 1.67 ± 0.01. Referring to Table I, the ratio of intercepts is 2.36 ± 0.19 for π^+ production and 3.08 ± 0.34 for π^- production, in substantial disagreement with the hypothesis of Pomeron factorization.

The difference of the π^+ and π^- induced cross sections should have a power-law dependence on s where the exponent is given by $\alpha_\rho(0) - 1 \approx -0.5$. These cross-section differences and fits to a power-law dependence are shown in Fig. 9 for π^-, π^+, and p production. The data are reasonably well fitted by a power law, but the effective intercepts, $\alpha(0) = 0.28 \pm 0.13$, 0.13 ± 0.17, and 0.19 ± 0.25, respectively, are considerably smaller than the value $\alpha(0) = 0.5$ which is expected for pure ρ-pole exchange.

Thus, although the data presented here are consistent with an approach to a scaling limit as $A + Bs^{-1/2}$, they are inconsistent in detail with the simplest Mueller-Regge phenomenology in which only the Pomeron and leading meson trajectories are considered. Bubble-chamber data at Fermilab energies indicate that in the kinematic region investigated here violations of Pomeron factorization are not large.[8] These data suggest further that the s dependence of the reaction $pp \to \pi^-$ is considerably more complicated than the simple form $A + Bs^{-1/2}$ found here.[9] Data from the CERN ISR (Ref. 10) on $pp \to \pi^{\pm}$ at $\sqrt{s} = 23.3$ GeV were integrated over the acceptance of the spectrometer and plotted in Figs. 8(a) and 8(b). These data confirm that the range of s in this experiment is too low to apply simple Mueller-Regge phenomenology. We, therefore, conclude that single-particle production is not well

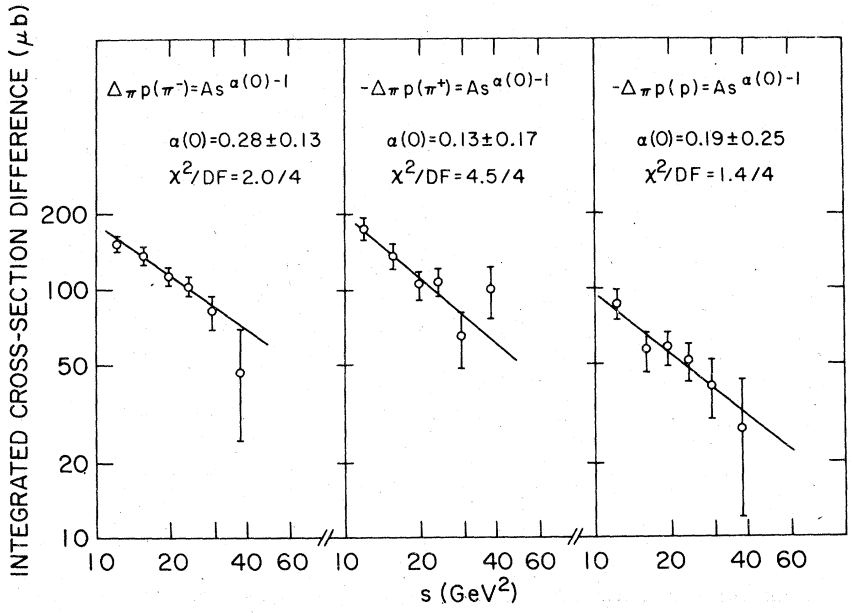

FIG. 9. Plots of the cross-section differences $\Delta_{\pi p}(c) = \Delta\sigma(\pi^- p \to c) - \Delta\sigma(\pi^+ p \to c)$ for $c = \pi^-$, π^+, and p. The solid lines are fits to $\Delta_{\pi p}(c) = As^{\alpha(0)-1}$.

described by simple Regge behavior in the range $4\ \mathrm{GeV}/c < p_a^{\mathrm{lab}} < 24\ \mathrm{GeV}/c$, in contradistinction to the total cross section in this momentum range.

Preliminary results[11] from a continuation of this experiment to Fermilab energies have shown that, when proper allowance is made for the s dependence of the cross sections, Pomeron factorization holds. In the following paper[6] further results from the study at higher energies are presented.

ACKNOWLEDGMENTS

We acknowledge the support of Rolf Brocker and James Cook in construction of the spectrometer and the support of the Brookhaven National Laboratory Accelerator Department and On-Line Data Facility in the execution of the experiment. This research was supported in part by the U. S. Department of Energy.

---

*Present address: TRW Systems, 7600 Colshire Drive, McLean, Virginia.

†Present address: Laboratory for Nuclear Studies, Cornell University, Ithaca, N.Y. 14853.

‡Present address: Accelerator Department, Brookhaven National Laboratory, Upton, New York 11973.

[1]R. P. Feynman, Phys. Rev. Lett. 23, 1415 (1969); J. Benecke, T. T. Chou, C. N. Yang, and E. Yen, Phys. Rev. 188, 2159 (1969). Representative reviews are H. Bøggild and T. Ferbel, Annu. Rev. Nucl. Sci. 24, 451 (1974), R. G. Roberts, in *Phenomenology of Particles at High Energies*, edited by R. L. Crawford and R. Jennings (Academic, London, 1974), and T. Ferbel, SLAC Report No. 179, 1974 (unpublished).

[2]A. H. Mueller, Phys. Rev. D 2, 2963 (1970).

[3]Chan Hong-Mo, C. S. Hsue, C. Quigg, and J.-M. Wang, Phys. Rev. Lett. 26, 672 (1971).

[4]D. Harting *et al.*, Nuovo Cimento 38, 60 (1965). Equally good agreement with A. R. Dzierba *et al.*, Phys. Rev. D 7, 725 (1973); is obtained, but is not shown for clarity.

[5]V. Blobel *et al.*, Nucl. Phys. B69, 454 (1974).

[6]H. Weisberg *et al.*, following paper, Phys. Rev. D 17, 2875 (1978).

[7]A. S. Carroll *et al.*, Phys. Lett. 61B, 303 (1976).

[8]J. Erwin *et al.*, Phys. Rev. Lett. 33, 1352 (1974).

[9]R. Schindler *et al.*, Phys. Rev. Lett. 33, 862 (1974); J. Whitmore *et al.*, Phys. Lett. 60B, 211 (1976); J. Whitmore *et al.*, Phys. Rev. Lett. 38, 996 (1977).

[10]P. Capiluppi *et al.*, Nucl. Phys. B79, 189 (1974).

[11]E. W. Beier *et al.*, Phys. Rev. Lett. 37, 1120 (1976).